Geophysical Research Letters

RESEARCH LETTER
10.1029/2021GL093861

# Small Shear Wave Splitting Delays Suggest Weak Anisotropy in Cratonic Mantle Lithosphere

**Xiaoran Chen**[1], **Vadim Levin**[1], **and Huaiyu Yuan**[2,3,4]

[1]Department of Earth and Planetary Sciences, Rutgers University, The State University of New Jersey, New Brunswick, NJ, USA, [2]Department of Earth and Environmental Sciences, ARC Centre of Excellence for Core to Crust Fluid Systems, Macquarie University, North Ryde, NSW, Australia, [3]Centre for Exploration Targeting, School of Earth Sciences, The University of Western Australia, Crawley, WA, Australia, [4]Geological Survey of Western Australia, Perth, WA, Australia

**Key Points:**

- Three consistent methods are used to measure splitting in core-refracted shear waves in Yilgarn and Superior cratons
- Small amount of splitting in both regions is found indicating weak anisotropy in both cratons' lithosphere
- Anisotropy in the asthenosphere likely contributes to splitting in the Superior but not in the Yilgarn

**Supporting Information:**

Supporting Information may be found in the online version of this article.

**Correspondence to:**

X. Chen,
xiaoran.chen@rutgers.edu

**Citation:**

Chen, X., Levin, V., & Yuan, H. (2021). Small shear wave splitting delays suggest weak anisotropy in cratonic mantle lithosphere. *Geophysical Research Letters*, *48*, e2021GL093861. https://doi.org/10.1029/2021GL093861

Received 14 APR 2021
Accepted 30 JUL 2021

**Abstract** We use splitting in core-refracted teleseismic shear waves (SKS, PKS, and similar) to investigate anisotropic properties of the upper mantle beneath the Superior craton in eastern North America and the Yilgarn craton in Western Australia. At four sites in each craton, we assemble extensive data sets that emphasize directional coverage, and use three different measurement methods to develop mutually consistent constraints on the nature of splitting and on the likely anisotropic properties that cause it. In both cratons, we see evidence of clear directional variation in both delays and fast polarization directions, as well as lateral differences between sites. Relatively small (0.3–0.8 s) amounts of splitting imply weak anisotropy within 150–220 km thick mantle lithosphere. Anisotropy in the asthenosphere likely contributes to splitting in North America where fast directions align with absolute plate motion, but not in Western Australia where fast polarizations and plate motion are nearly orthogonal.

**Plain Language Summary** Cratons, areas of the continents that did not deform for a billion years or more, are the only record of the geological events from the first half of Earth's existence. Large-scale deformation of the rigid lithosphere of cratons is expected to imprint a systematic fabric within its rocks. This fabric makes the speed of seismic waves dependent on direction (anisotropic) and causes birefringence (splitting) in horizontally polarized (shear) waves from distant earthquakes. Surprisingly low level of birefringence is seen in many cratons, suggesting weak anisotropy and by inference—a poorly developed systematic fabric within them. Alternatively, competing effects of fossil anisotropy in the lithosphere and the anisotropy due to present-day deformation beneath it can result in cancellation of birefringence. We measured splitting in large data sets from the Yilgarn craton of Western Australia and the Superior craton in eastern North America. We confirm the small amount of splitting in both areas and rule out mutually canceling effects of anisotropy within and beneath the lithosphere. This suggests weak anisotropy in the lithosphere of both cratons. Directions of tectonic plate motion suggest that anisotropy due to deformation beneath the lithosphere affects our measurements in North America but not in Australia.

## 1. Introduction

Cratons are large domains of continental crust, which have experienced little internal deformation and have maintained long-term stability since their formation during the Archean epoch. Most cratons are composed of numerous distinct terranes formed relatively early in Earth's history and are assembled by processes that continue being debated (Hawkesworth et al., 2017; Lee et al., 2011; Percival et al., 2012; Wyman & Kerrich, 2009).

Seismic anisotropy, the dependence of seismic velocity on the direction of wave propagation, is a proxy for deformation in the interior of the Earth (Silver, 1996). Past tectonic episodes are likely to leave their record in the anisotropic structure of continental lithosphere (Long & Becker, 2010). Observations of birefringence (splitting) in core-refracted shear waves (e.g., an SKS phase) attest to the common presence of anisotropy in the upper mantle (Savage, 1999; Vinnik et al., 1984), with a global average splitting time of ∼1 s (Silver, 1996; Figure S1).

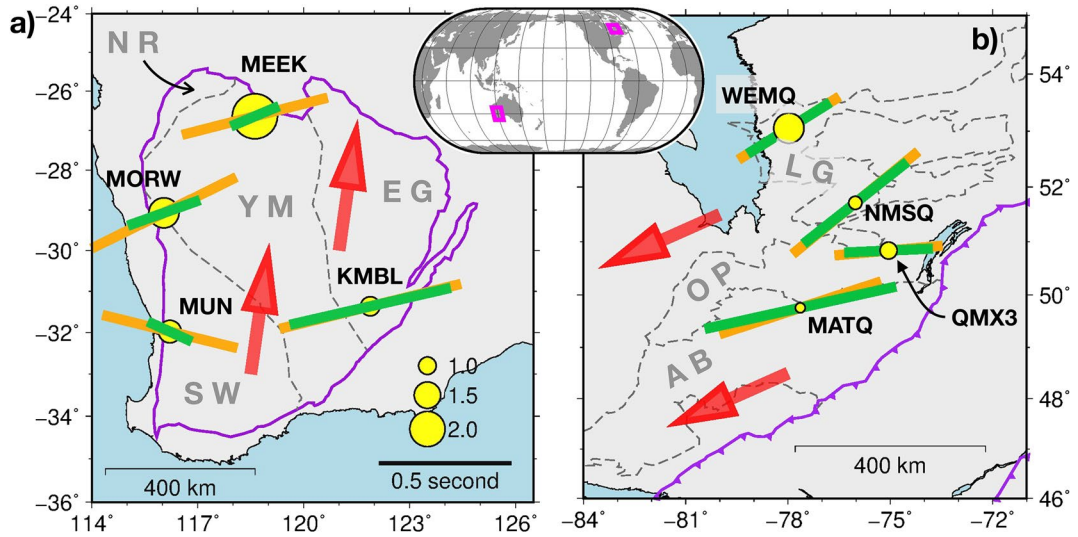


**Figure 1.** Tectonic elements, plate motions, and average measurements. Inset shows locations of two areas. Red arrows—plate motion directions in NUVEL-HS3 reference frame. Splitting measurements (sticks aligned with fast polarization and scaled with delay) are shown at corresponding sites (labeled): site averages $\varphi_a$ and $\delta_a$—green, best-fit values $\varphi_f$ and $\delta_f$—orange, and $R_{\mathrm{NULL}}$—yellow circles. See Section 2 for definitions of parameters. Tectonic units: (a) Yilgarn: NR—Narryer Terrane, SW—Southwestern Terrane, EG—Eastern Goldfields Super-terrane, and YM—Youanmi terrane; (b) Superior: LG—La Grande Subprovince, OP—Opatica Subprovince, and AB—Abitibi Terrane.

Despite their long histories, some cratons exhibit low levels of shear wave splitting (Chen et al., 2018; Heintz & Kennett, 2005; Silver et al., 2001). However, existing studies are often limited in the number of measurements and the range of wave propagation directions. Observations of splitting in shear waves are expected to vary directionally when the anisotropic structure is complex (Levin et al., 1999; Long & Silver, 2009; Silver & Savage, 1994), making interpreted anisotropic structures beneath cratons less certain. In particular, multiple layers of different anisotropy beneath cratons (Debayle et al., 2005; Gung et al., 2003; Yuan & Romanowicz, 2010) can result in apparently weak shear wave splitting signal. Records of core refracted waves from multiple directions are needed to resolve the ambiguity making multi-year observing periods necessary.

Weak splitting was previously reported in the Yilgarn craton in Western Australia (Heintz & Kennett, 2005) and the eastern Superior craton in North America (Chen et al., 2018; Darbyshire et al., 2015). The 2.6 Ga old Yilgarn craton (Champion & Smithies, 2007; Griffin et al., 2004; Figure 1a) includes terranes as old as 3.8 Ga. While subduction-like processes likely shaped the Eastern Goldfields terrane, both plumes and subduction episodes were proposed for others (Czarnota et al., 2010; Van Kranendonk et al., 2013; Wyman, 2019). Consolidated at nearly the same time, the Superior craton consists of lithologically and structurally distinct linear subprovinces (Card, 1990; Percival, 2007). Percival et al. (2012) proposed subduction as the main agent of Superior craton formation, although alternative views do exist (e.g., Bedard & Harris, 2014). The Yilgarn and Superior cratons did not come into contact during the supercontinental assemblies of Pangea (Muttoni et al., 2009), Rodinia (Y. Li et al., 2008), and Nuna/Columbia (Nance et al., 2014). Their independent formation and evolution paths make them good locations to perform comparative studies of cratonic lithosphere.

We develop detailed descriptions of shear wave splitting patterns in the Superior and Yilgarn cratons. Using data from long-operating sites, we apply three mutually consistent methods to evaluate directionally variable splitting in multiple types of core-refracted waves. We confirm the overall finding of a very weak splitting signal and argue that it most likely reflects the absence of strongly developed fabric in the mantle lithosphere of these cratons.

## 2. Methods

Shear wave splitting methods using records of individual seismic phases (Silver & Chan, 1991; Vinnik et al., 1984) estimate apparent anisotropy along their raypaths. The drawbacks of this approach, such as the disagreement between different algorithms, and the systematic failures of measurements near the true fast polarizations are well documented (e.g., Wüstefeld & Bokelmann, 2007). We follow procedures described and illustrated in Chen et al. (2018) and Li et al. (2019), and summarize technical details in Text S1. Specifically, we combine insights from multiple measurements on single records with results from two other techniques: measurements of splitting intensity (SI) (Chevrot, 2000) and inversion for anisotropy parameters in a single layer of anisotropy (Menke & Levin, 2003). All three techniques represent the real anisotropic structure beneath an area by a single anisotropic layer with a horizontal symmetry axis. The first two methods provide estimates of "apparent" splitting parameters for the chosen location while the third adds an extra constraint on the "average" anisotropic properties within an anisotropic layer, subject to geometric assumptions. Thus, the single-phase measurements make sure that we make a thorough examination of all the data available at a site, while the integration of three methodologies documented in the paper gives us extra confidence in our interpretation.

Primary parameters produced by our analysis are (a) fast polarization directions, splitting delays, and SI values for individual shear wave records, (b) site-average values of fast polarization $\varphi_a$ and delay $\delta_a$ obtained separately for delays and fast polarizations of all non-NULL measurements (Text S1), (c) best-fit values of fast polarization $\varphi_f$ and delay $\delta_f$ calculated from the directional dependence of SI values, and (d) orientation of the horizontal fast symmetry axis $\varphi_s$ and the strength of anisotropy in a layer. Given a full trade-off between anisotropy strength and layer thickness, we fix the latter at 100 km. We compute a ratio of counts of NULL and non-NULL measurements for each site ($R_{\mathrm{NULL}}$), and evaluate delay predicted for a vertically propagating $S$ wave in the layer with anisotropy strength determined by the inversion. Taken together, these internally consistent metrics provide a more nuanced description of the anisotropic properties beneath the sites we have studied and make the comparisons of different locations more meaningful.

## 3. Data

The areas we investigate have few long-operating seismic stations. In this study, we focus on a detailed and thorough analysis of data only at representative sites with high quality data and good directional coverage (see Text S2 for the site selection). We chose four locations per craton, each within a different terrane, thus probing the lithosphere with a different history. In the Yilgarn craton, we use records from 55 earthquakes between 2010 and 2019 with magnitudes above 6 (Figure S3a) recorded at stations KMBL, MEEK, MORW, and MUN (Australian National Seismograph Network, http://ds.iris.edu/mda/AU, Table S1). In the Superior craton, we use permanent stations MATQ, NMSQ, and WEMQ (POLARIS stations in Quebec, http://ds.iris.edu/mda/PO, Table S1) and temporary sites QM76, QM78, and QM80 (QMIII Flexible Array, http://ds.iris.edu/mda/X8) separated by distances ~20 km, which we combined into a composite location "QMX3." We use records from 144 earthquakes between 2005 and 2015 with magnitudes above 5.5 (Figure S3b). A subset of records from "QMX3" location was discussed in Chen et al. (2018), which provided illustrations of waveforms and measurement procedures.

## 4. Results

We document our results for the sites with representative patterns of shear wave splitting (two per craton, Figure 2). Other sites are shown in the supplement, along with a table containing all the measurements for individual records. In Table 1, we present values for average and best-fit values for all sites.

### 4.1. Yilgarn Craton

We obtained 223 (62 PKS + 53 SKS + 104 SKKS + 4 SKiKS) new measurements of shear wave splitting and SI, with 45–65 measurements per site. Of these, 85 are non-NULL splitting measurements and 138 are NULL measurements (Table S1).

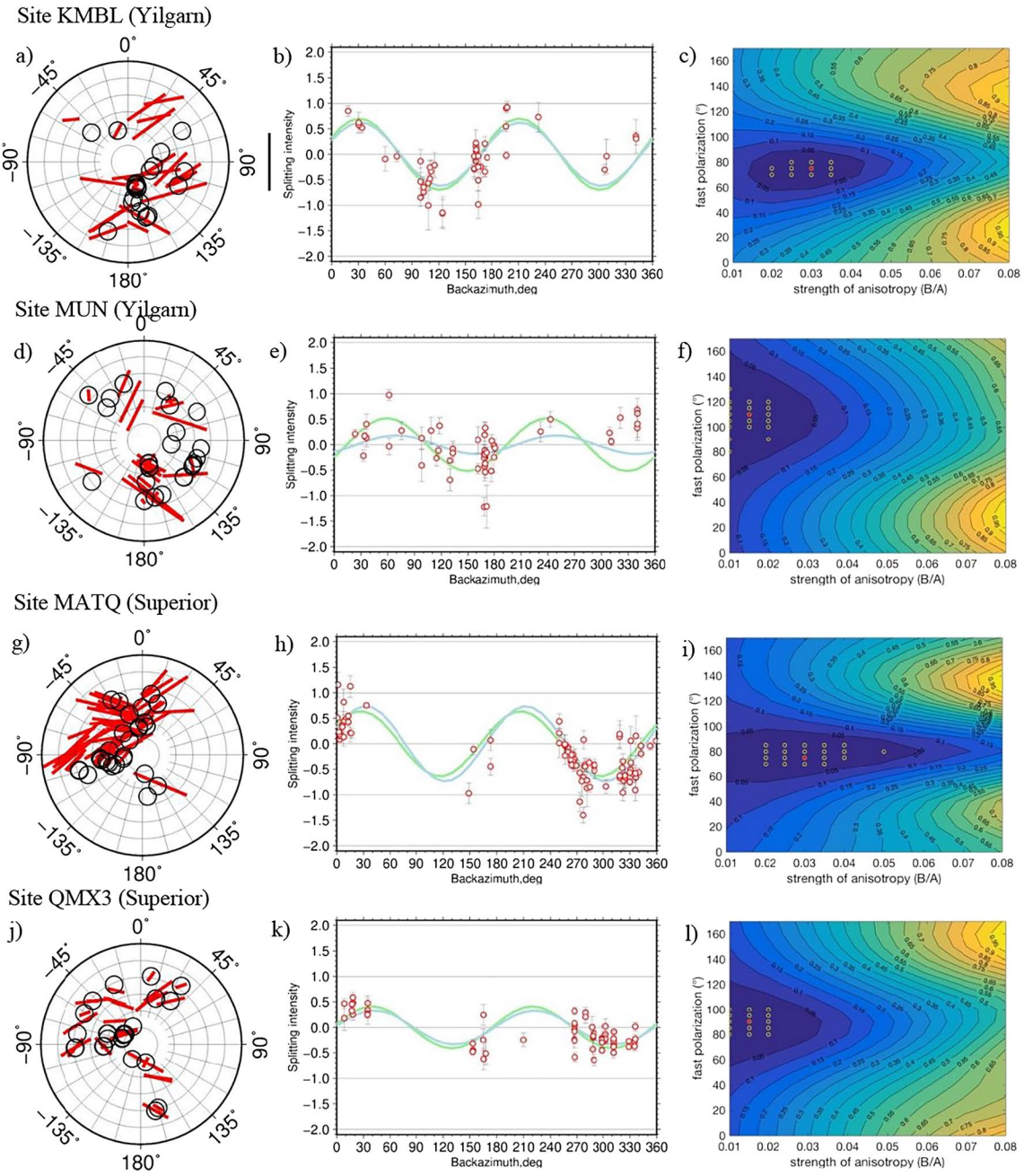


**Figure 2.** Measurements for representative sites KMBL, MUN, MATQ, and QMX3 (see Figure 1 for locations). Parts (a, d, g, and j) are stereo-plots of all splitting measurements (red bars aligned with fast polarization, North is up, scaled with delay) and NULL observations (circles) plotted according to their rays back azimuths (positive clockwise from 0° to 360°, grid step 15°) and incident angles (increasing from 0° at the center to 18° at the edge of the plot, grid step 3°). Black bar to the right of (a) shows 1 s scale. Parts (b, e, h, and k) are splitting intensity measurements (red circles with 95% confidence intervals) and sinusoid functions fitted to them (blue) and predicted based on $\varphi_a$ and $\delta_a$ for the site (green). Parts (c, f, i, and l) are normalized error surfaces of the parameter search for the strength of anisotropy (%) and the azimuths of the fast axis $\varphi_s$. Contours are spaced at 5% of the full error range. Yellow circles represent parameter combinations with errors within 2% of the best-fitting combination (red asterisk).

Averaged splitting parameters are similar at KMBL, MEEK, and MORW (Table S1), with $\varphi_a = 76°$, 76°, and 64° respectively, whereas at site MUN $\varphi_a = 104°$, which is ~30° different. We can observe directional variations of fast polarization at all four sites (Figures 2 and S3). Average delays are relatively consistent, with $\delta_a$ between 0.5 and 0.7 s at all sites. In addition, at each individual site, we have a large number of NULL

**Table 1**
*Measurements and Selected Information for Individual Sites*

| | $\varphi_a$ | $\delta_a$ | $\varphi_f$ | $\delta_f$ | $\varphi_s$ | $\delta_s$ | $\delta_s$ | $R_{\mathrm{NULL}}$ | APM |
|---|---|---|---|---|---|---|---|---|---|
| **Yilgarn** | | | | | | | | | |
| KMBL | 76° | 0.7 s | 76° | 0.6 s | 75° | 3% | 0.75 s | 1.1 | 6° |
| MEEK | 76° | 0.6 s | 68° | 0.2 s | 75° | 2% | 0.50 s | 2.6 | 7° |
| MORW | 64° | 0.6 s | 71° | 0.3 s | 70° | 2% | 0.50 s | 1.7 | 9° |
| MUN | 104° | 0.5 s | 113° | 0.2 s | 110° | 1.5% | 0.375 s | 1.3 | 10° |
| **Superior** | | | | | | | | | |
| MATQ | 72° | 0.6 s | 78° | 0.7 s | 75° | 3% | 0.75 s | 0.6 | 247° |
| NMSQ | 51° | 0.6 s | 50° | 0.5 s | 50° | 2.5% | 0.625 s | 0.7 | 246° |
| WEMQ | 58° | 0.5 s | 58° | 0.4 s | 60° | 1.5% | 0.375 s | 1.7 | 245° |
| QMX3 | 85° | 0.4 s | 87° | 0.3 s | 90° | 1.5% | 0.375 s | 1.0 | 247° |

*Note.* $\varphi_a$ and $\delta_a$: averaged observed splitting parameters, and $\delta_f$: splitting parameters estimated using a weighted SI; $\varphi_s$ and $\delta_s$, splitting parameters estimated from the best-fitting model in single-layer inversion, percentage of anisotropy $\delta_s$ (%) is unitless, $\delta_s$ (s) is an equivalent of $\delta_s$ (%) in seconds; $R_{\mathrm{NULL}}$: fraction of NULL measurements; APM in NUVEL1A-HS3 model.

Abbreviations: APM, absolute plate motion; SI, splitting intensity.

measurements that can be observed from nearly all back azimuths. All four sites have $R_{\mathrm{NULL}}$ values above 1, with KMBL being the smallest of just above 1, and MEEK the largest with 2.6.

At all sites, SI measurements fall within ±1 s, with most being close to 0 (Figures 2 and S3). Values of $\delta_f$ are in the range of 0.2–0.6 s, and systematically smaller when compared with the corresponding $\delta_a$ values, with KMBL having the closest match with $\delta_f = 0.6$ s and MUN the largest mismatch with $\delta_f = 0.2$ s (Figure 2). Fast polarization values match within 10° at all sites (Table 1).

Results from single-layer inversions (Figures 2c and 2e) show a good agreement with the other two methods, with best-fit $\varphi_s$ values within 10° of both site average and best-fit values, and predicted delays $\delta_s$ in the range 0.4–0.8 s. The error surface plots show that a range of fast polarizations within ±15° of the best value fit the data equally well, and also suggest that significant anisotropy is required at site KMBL only, with a best fit of 3% within 100 km. At the other three sites data are fit well with anisotropy strength of 1% or even lower.

### 4.2. Superior Craton

We made 263 (34 PKS + 134 SKS + 69 SKKS + 1 PKIKS + 25 SKiKS) measurements of shear wave splitting and SI, with 142 non-NULL splitting measurements and 121 NULL measurements. Individual sites have 47–87 measurements (Table S1). All four sites have similar averaged splitting parameters, with $\varphi_a = 50°–85°$ and $\delta_a$ between 0.4 to 0.6 s (Table 1). Directional variations of fast polarization directions measured from individual records and NULL measurements from nearly all back azimuths are found at all sites. $R_{\mathrm{NULL}}$ values are not as high as in the Yilgarn craton, ranging from 0.6 at site MATQ to 1.7 at site WEMQ. SI measurements are largely within 1 s at all locations. Their directional patterns yield $\delta_f$ estimates within 0.1 s of corresponding $\delta_a$ values, and fast polarization estimates $\varphi_f$ are within 5° of the corresponding $\varphi_a$ values (Table 1). Results from single-layer inversions (Figures 2i and 2l) show a good agreement with the other two methods. Best estimates of the fast symmetry axis orientation values are within 5° of both $\varphi_f$ and $\varphi_a$ for their respective sites, and estimates of $\delta_s$ for best-fitting anisotropy strength values are within 0.1 s of $\delta_a$ and $\delta_f$. Ranges of acceptable values in error surfaces are fairly large. At site MATQ in particular, both very small amounts of anisotropy and values up to 5% fit data equally well, suggesting a relatively poor constraint on this parameter in the inversion. At other sites, maximum possible anisotropy strength is lower. Orientations of fast axes are constrained within a range of ±15°.

### 4.3. Comparison Between Yilgarn and Superior Craton

The cratons we studied show considerable similarity in the nature of shear wave splitting observations. At all sites, we find evidence for birefringence in core-refracted shear waves. The average delay values are between 0.3 and 0.8 s, significantly smaller than the global average of ∼1 s (Long & Silver, 2009; Silver, 1996; Figure S1). NULL observations are present at all sites as well, and often from the same directions as observations yielding reliable estimates of splitting parameters. At some locations, there are more NULL observations than non-NULL measurements. Fast polarization directions vary with backazimuths at all sites. Neither craton has a uniform pattern of shear wave splitting, with both delays and fast polarization orientations at individual sites within each craton varying over distances of a few hundreds of kilometers. Both cratons have locations where the amounts of splitting are relatively large (KMBL in the Yilgarn, MATQ and NMSQ in the Superior), and also sites where they are very small (MUN in the Yilgarn, QMX3 and WEMQ in the Superior).

One distinction is that the sites in the Superior show a high degree of internal consistency for the three methods, while in the Yilgarn there are noticeable differences in values of $\delta_a$ and $\delta_f$ at all sites except KMBL. Correspondingly, high values of $R_{\mathrm{NULL}}$ in the Yilgarn suggest that the difference stems from the inclusion of records that yield NULL splitting observations in the $\delta_f$ estimate.

## 5. Discussion

### 5.1. Comparison With Previous Studies

Previous studies of shear wave splitting find delays of 1 s or less in the Superior craton (e.g., Chen et al., 2018; Darbyshire et al., 2015; Frederiksen et al., 2007; Rondenay et al., 2000). In the Yilgarn craton splitting delays ranked "good" by Heintz and Kennett (2005) also are under 1 s, and a large fraction of measurements consist of NULL results. Comparison of average fast polarization directions is complicated by differences in the sets of data included by various studies, especially those of Rondenay et al. (2000) and Heintz and Kennett (2005) where observations were collected over only a few months.

A significant improvement of our study is that we use long (up to 10 years) observing periods, emphasizing a nearly full coverage of possible back azimuths. In this way, small delay times in our individual measurements are not biased by preferential observation of certain directions. Moreover, besides the commonly used SKS and SKKS phases, we also include phases such as PKS, SKKS, and SKiKS, broadening the range of ray parameters. Multi-year observing periods and inclusion of additional phases make directional variations in apparent fast polarizations more obvious at some of the sites (e.g., MATQ, Figures 2 and S5) while there is no apparent pattern at others (e.g., MUN and QMX3).

Studies using surface waves on global and regional scales suggest that the upper mantle is both radially and azimuthally anisotropic beneath both the Yilgarn and the Superior cratons (Darbyshire & Lebedev, 2009; Debayle et al., 2005, 2016; Lebedev et al., 2009; Petrescu et al., 2017; Simons & van der Hilst, 2003; Yoshizawa & Kennett, 2015; Yuan et al., 2011). Both the magnitude of anisotropy and the orientation of fast shear wave polarization vary with depth, raising the possibility that multiple layers of different anisotropic properties provide mutually canceling contributions to the vertically integrated shear wave splitting signal. Recognizing that lateral resolution of most surface wave models is not sufficient to isolate upper mantle volumes affecting individual sites, we note that reported fast shear wave directions are not truly orthogonal beneath either the Superior (Petrescu et al., 2017; Yuan et al., 2011) or the Yilgarn craton (Simons & van der Hilst, 2003). Furthermore, to cancel the splitting in every terrane of the Yilgarn craton, lithospheric fabrics inherited from tectonic events 2.6 Ga or older need to match the current deformation in the asthenosphere very closely.

### 5.2. Shear Wave Splitting Results in the Geodynamic Context of Two Cratons

The shearing of the asthenosphere by the motion of tectonic plates is a likely source of anisotropy in the mantle and thus has to be reflected by the splitting of shear waves (Long & Silver, 2009). We compare averaged fast polarizations with absolute plate motion (APM) directions in the NUVEL1A-HS3 model (Figure 1 and Table 1). In the Superior craton, the averaged fast polarizations generally align well with the APM

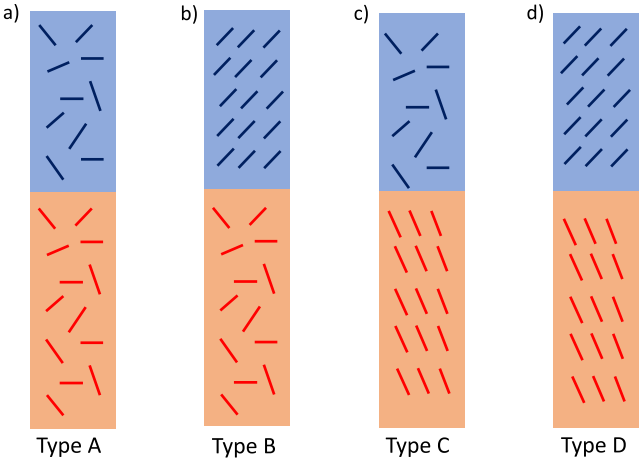


**Figure 3.** Possible scenarios of rock fabric beneath cratons. Blue and orange rectangles stand for the lithosphere and the asthenosphere, while short sticks stand for different kinds of fabrics in the mantle. Type A has no systematic fabric either in the lithosphere or in the asthenosphere, whereas Type D has systematic fabric in both the lithosphere and asthenosphere. Types B and C only have systematic fabric in the lithosphere and asthenosphere correspondingly.

direction, while at all sites in the Yilgarn craton, the averaged fast polarizations and the directions of the plate motion are nearly orthogonal. This disparity is especially puzzling in view of the fast rate of the Australian plate motion, and the insight from a global survey of continents by Debayle et al. (2005) that only beneath Australia is the fast polarization of shear wave speed in the asthenosphere consistent with the expected plate motion direction. A pertinent difference between the Superior and the Yilgarn cratons may be their lithospheric thickness relative to the adjacent regions. While the oldest parts of the Superior craton are among the thickest lithosphere of the North America craton but with a relatively flat lithosphere-asthenosphere-boundary (LAB) (Yuan & Romanowicz, 2010), the Yilgarn lithosphere is thinner than the areas to its east and the secondary variation to the LAB depth in the Yilgarn craton is present (e.g., Simons et al., 2002; Yoshizawa & Kennett, 2015). As Australia moves rapidly northward (Figure 1), this local LAB topography variation may possibly result in a complex pattern of mantle flow. Indeed, a more localized study by Simons and van der Hilst (2003) shows laterally variable fast polarization directions at sub-crustal lithospheric depths.

### 5.3. An Argument for Weak Anisotropy in the Cratonic Mantle Lithosphere

At all sites in two cratons with independent tectonic histories, we observe small splitting delays and large fractions of NULL measurements. Moreover, all sites show directional variation of fast polarizations, and lateral differences in splitting patterns can be observed within each craton. For instance, sites MUN in the Yilgarn craton and QMX3 in the Superior craton have small delays and scattered fast polarizations, whereas sites KMBL in the Yilgarn craton and MATQ and NMSQ in the Superior craton show larger delays and more consistent directionally varying fast polarizations. Notably, in all cases, the total amount of splitting is significantly smaller than the global average value (Figure S1) or the values found in the immediately adjacent regions with younger lithosphere (e.g., Chen et al., 2018). Given that the mantle lithosphere beneath the regions we have studied extends to depths of 150–220 km, the vertically integrated strength of anisotropy within it cannot be large. Indeed, the notion of weak anisotropy in the lithosphere of the eastern Superior craton is in good agreement with low levels of azimuthal anisotropy of phase velocity of Rayleigh waves with periods of 140 s and shorter (Petrescu et al., 2017, see Figure S6), as well as the weak lithospheric SKS splitting predicted in the surface wave model of Yuan et al. (2011).

Lateral changes in the nature of shear wave splitting parameters on scales of hundreds of kilometers suggest varying degrees of systematic rock fabric within the mantle lithosphere of individual cratons. Figure 3 shows four general scenarios of rock fabric beneath cratons, each corresponding to one or more locations we have explored. Locations in the Yilgarn craton likely do not reflect a contribution from the deforming asthenosphere (Figures 3a and 3b). Site KMBL shows clear evidence of splitting well matched by a single layer of anisotropy that we believe reflects the nature of the relatively young Eastern Goldfields super-terrane hosting it (Figure 3b). Other locations in the Yilgarn reside in older terranes (Czarnota et al., 2010), and their splitting patterns imply weakly developed, or absent, systematic fabric in the lithosphere (Figure 3a). Site MUN presents an especially complicated pattern possibly affected by its location close to the edge of the craton; however, the regional tomographic model of Yoshizawa (2014) does show a rather uniformly high-velocity lithospheric lid there.

In the Superior craton, average fast polarizations are nearly aligned with the APM (Figure 1), which makes a contribution of anisotropy from shearing of the asthenosphere likely (Figures 3c and 3d). Sites MATQ and NMSQ have relatively larger delays and show clear directional variations of fast polarizations (Figures 2 and S7), which may reflect an additional contribution of anisotropy from the internal fabric preserved in

the lithosphere of their respective terranes (Figure 3d). This contribution is less obvious at the other two locations, WEMQ and QMX3, where well developed fabric in the lithosphere is unlikely (Figure 3c).

In summary, we examined patterns of shear wave splitting in two cratons that formed and evolved far apart, paying special attention to directional variations of observed signals, and employing multiple methods to evaluate the amount of splitting. Consistently small splitting delay values we documented in both locations suggest weak anisotropy within their lithosphere, a feature that may be common to all cratons.

## Data Availability Statement

All data can be accessed at the Data Management Center (DMC) of the Incorporated Research Institutions for Seismology (IRIS) and Portable Observatories for Lithospheric Analysis and Research Investigating Seismicity (http://ds.iris.edu/mda/PO). Figures are drafted using GMT (Wessel & Smith, 1991) and Matlab (R2016a).

**Acknowledgments**
This work was supported by the NSF Earthscope grants EAR-1147831 and 1735912, the graduate fellowship and the Off-Campus Dissertation Development Awards provided by the School of Graduate Studies of Rutgers, the State University of New Jersey for the first author. Xiaoran Chen acknowledges the sponsorship from the CCFS, Macquarie University, and the CET, UWA. Huaiyu Yuan acknowledges partial support from the NSFC grant 91955210 and the Western Australian Exploration Incentive Scheme (EIS). This is contribution 1672 from the ARC Centre of Excellence for Core to Crust Fluid Systems (http://www.ccfs.mq.edu.au).

## References

Bédard, J. H., & Harris, L. B. (2014). Neoarchean disaggregation and reassembly of the Superior craton. *Geology*, *42*(11), 951–954. https://doi.org/10.1130/G35770.1

Card, K. D. (1990). A review of the superior province of the Canadian Shield, a product of Archean accretion. *Precambrian research*, *48*(1-2), 99–156. https://doi.org/10.1016/0301-9268(90)90059-y

Champion, D. C., & Smithies, R. H. (2007). Chapter 4.3: Geochemistry of Paleoarchean granites of the East Pilbara Terrane, Pilbara Craton, Western Australia: Implications for early Archean crustal growth. In M. J. van Kranendonk, R. H. Smithies, & V. C. Bennett (Eds.), *Developments in Precambrian geology* (Vol. 15, pp. 369–409). Elsevier. https://doi.org/10.1016/s0166-2635(07)15043-x

Chen, X., Li, Y., & Levin, V. (2018). Shear wave splitting beneath Eastern North American continent: Evidence for a multilayered and laterally variable. *Anisotropic Structure*, *19*(8), 2857–2871. https://doi.org/10.1029/2018gc007646

Chevrot, S. (2000). Multichannel analysis of shear wave splitting. *Journal of Geophysical Research*, *105*(B9), 21579–21590. https://doi.org/10.1029/2000jb900199

Czarnota, K., Champion, D. C., Goscombe, B., Blewett, R. S., Cassidy, K. F., Henson, P. A., & Groenewald, P. B. (2010). Geodynamics of the eastern Yilgarn Craton. *Precambrian Research*, *183*(2), 175–202. https://doi.org/10.1016/j.precamres.2010.08.004

Darbyshire, F., & Lebedev, S. (2009). Rayleigh wave phase-velocity heterogeneity and multilayered azimuthal anisotropy of the Superior Craton, Ontario. *Geophysical Journal International*, *176*(1), 215–234. https://doi.org/10.1111/j.1365-246x.2008.03982.x

Darbyshire, F. A., Bastow, I., Forte, A., Hobbs, T., Calvel, A., Gonzalez-Monteza, A., & Schow, B. (2015). Variability and origin of seismic anisotropy across eastern Canada: Evidence from shear wave splitting measurements. *Journal of Geophysical Research: Solid Earth*, *120*(12), 8404–8421. https://doi.org/10.1002/2015jb012228

Debayle, E., Dubuffet, F., & Durand, S. (2016). An automatically updated S-wave model of the upper mantle and the depth extent of azimuthal anisotropy. *Geophysical Research Letters*, *43*(2), 674–682. https://doi.org/10.1002/2015gl067329

Debayle, E., Kennett, B., & Priestley, K. (2005). Global azimuthal seismic anisotropy and the unique plate-motion deformation of Australia. *Nature*, *433*(7025), 509–512. https://doi.org/10.1038/nature03247

Frederiksen, A., Miong, S. K., Darbyshire, F., Eaton, D., Rondenay, S., & Sol, S. (2007). Lithospheric variations across the Superior Province, Ontario, Canada: Evidence from tomography and shear wave splitting. *Journal of Geophysical Research*, *112*(B7). https://doi.org/10.1029/2006jb004861

Griffin, W. L., O'Reilly, S. Y., Doyle, B. J., Pearson, N. J., Coopersmith, H., Kivi, K., et al. (2004). Lithosphere mapping beneath the North American plate. *Lithos*, *77*(1), 873–922. https://doi.org/10.1016/j.lithos.2004.03.034

Gung, Y., Panning, M., & Romanowicz, B. (2003). Global anisotropy and the thickness of continents. *Nature*, *422*(6933), 707–711. https://doi.org/10.1038/nature01559

Hawkesworth, C. J., Cawood, P. A., Dhuime, B., & Kemp, T. I. S. (2017). Earth's continental lithosphere through time. *Annual Review of Earth and Planetary Sciences*, *45*(1), 169–198. https://doi.org/10.1146/annurev-earth-063016-020525

Heintz, M., & Kennett, B. L. N. (2005). Continental scale shear wave splitting analysis: Investigation of seismic anisotropy underneath the Australian continent. *Earth and Planetary Science Letters*, *236*(1), 106–119. https://doi.org/10.1016/j.epsl.2005.05.003

Lebedev, S., Boonen, J., & Trampert, J. (2009). Seismic structure of Precambrian lithosphere: New constraints from broad-band surface-wave dispersion. *Lithos*, *109*(1), 96–111. https://doi.org/10.1016/j.lithos.2008.06.010

Lee, C.-T. A., Luffi, P., & Chin, E. J. (2011). Building and destroying continental mantle. *Annual Review of Earth and Planetary Sciences*, *39*(1), 59–90. https://doi.org/10.1146/annurev-earth-040610-133505

Levin, V., Menke, W., & Park, J. (1999). Shear wave splitting in the Appalachians and the Urals: A case for multilayered anisotropy. *Journal of Geophysical Research*, *104*(B8), 17975–17993. https://doi.org/10.1029/1999jb900168

Li, Y., Levin, V., Elkington, S., & Hlavaty, J. (2019). Localized anisotropic domains beneath Eastern North America. *Geochemistry, Geophysics, Geosystems*, *20*(11), 5499–5521. https://doi.org/10.1029/2019gc008518

Li, Z. X., Bogdanova, S., Collins, A., Davidson, A., De Waele, B., Ernst, R., et al. (2008). Assembly, configuration, and break-up history of Rodinia: A synthesis. *Precambrian Research*, *160*(1), 179–210. https://doi.org/10.1016/j.precamres.2007.04.021

Long, M. D., & Becker, T. W. (2010). Mantle dynamics and seismic anisotropy. *Earth and Planetary Science Letters*, *297*, 341–354. https://doi.org/10.1016/j.epsl.2010.06.036

Long, M. D., & Silver, P. G. (2009). Shear wave splitting and mantle anisotropy: Measurements, interpretations, and new directions. *Surveys in Geophysics*, *30*(4–5), 407–461. https://doi.org/10.1007/s10712-009-9075-1

Menke, W., & Levin, V. (2003). The cross-convolution method for interpreting SKS splitting observations, with application to one and two-layer anisotropic earth models. *Geophysical Journal International*, *154*(2), 379–392. https://doi.org/10.1046/j.1365-246X.2003.01937.x

Muttoni, G., Gaetani, M., Kent, D. V., Sciunnach, D., Angiolini, L., Berra, F., et al. (2009). Opening of the Neo-Tethys Ocean and the Pangea B to Pangea A transformation during the Permian. *GeoArabia*, *14*(4), 17–48.

Nance, R. D., Murphy, J. B., & Santosh, M. (2014). The supercontinent cycle: A retrospective essay. *Gondwana Research*, *25*(1), 4–29. https://doi.org/10.1016/j.gr.2012.12.026

Percival, J. A. (2007). *Mineral deposits of Canada: A synthesis of major deposit-types, district metallogeny, the evolution of geological provinces, and exploration methods* (pp. 903–928). Geology and Metallogeny of the Superior Province.

Percival, J. A., Skulski, T., Sanborn-Barrie, M., Stott, G. M., Leclair, A. D., Corkery, M. T., & Boily, M. (2012). Geology and tectonic evolution of the Superior Province, Canada. In Tectonic styles in Canada: The LITHOPROBE perspective (Vol. 49, pp. 321–378). Geological Association of Canada.

Petrescu, L., Darbyshire, F., Bastow, I., Totten, E., & Gilligan, A. (2017). Seismic anisotropy of Precambrian lithosphere: Insights from Rayleigh wave tomography of the eastern Superior Craton. *Journal of Geophysical Research: Solid Earth*, *122*(5), 3754–3775. https://doi.org/10.1002/2016jb013599

Rondenay, S., Bostock, M. G., Hearn, T. M., White, D. J., Wu, H., Sénéchal, G., et al. (2000). Teleseismic studies of the lithosphere below the Abitibi-Grenville Lithoprobe transect. *Canadian Journal of Earth Sciences*, *37*(2–3), 415–426. https://doi.org/10.1139/e98-088

Savage, M. (1999). Seismic anisotropy and mantle deformation: What have we learned from shear wave splitting? *Reviews of Geophysics*, *37*(1), 65–106. https://doi.org/10.1029/98rg02075

Silver, P. G. (1996). Seismic anisotropy beneath the continents: Probing the depths of geology. *Annual Review of Earth and Planetary Sciences*, *24*(1), 385–432. https://doi.org/10.1146/annurev.earth.24.1.385

Silver, P. G., & Chan, W. W. (1991). Shear-wave splitting and subcontinental mantle deformation. *Journal of Geophysical Research*, *96*(B10), 16429–16454. https://doi.org/10.1029/91jb00899

Silver, P. G., Gao, S. S., Liu, K. H., & Group, K. S. (2001). Mantle deformation beneath southern Africa. *Geophysical Research Letters*, *28*(13), 2493–2496. https://doi.org/10.1029/2000gl012696

Silver, P. G., & Savage, M. K. (1994). The Interpretation of shear-wave splitting parameters in the presence of two anisotropic layers. *Geophysical Journal International*, *119*(3), 949–963. https://doi.org/10.1111/j.1365-246X.1994.tb04027.x

Simons, F. J., & van der Hilst, R. D. (2003). Seismic and mechanical anisotropy and the past and present deformation of the Australian lithosphere. *Earth and Planetary Science Letters*, *211*(3), 271–286. https://doi.org/10.1016/s0012-821x(03)00198-5

Simons, F. J., van der Hilst, R. D., Montagner, J.-P., & Zielhuis, A. (2002). Multimode Rayleigh wave inversion for heterogeneity and azimuthal anisotropy of the Australian upper mantle. *Geophysical Journal International*, *151*(3), 738–754. https://doi.org/10.1046/j.1365-246X.2002.01787.x

Van Kranendonk, M. J., Ivanic, T. J., Wingate, M. T. D., Kirkland, C. L., & Wyche, S. (2013). Long-lived, autochthonous development of the Archean Murchison Domain, and implications for Yilgarn Craton tectonics. *Precambrian Research*, *229*, 49–92. https://doi.org/10.1016/j.precamres.2012.08.009

Vinnik, L., Kosarev, G., & Makeeva, L. (1984). Lithosphere anisotropy from the observation of SKS and SKKS waves. *Doklady Akademii Nauk SSSR*, *278*(6), 1335–1339.[in Russian]

Wessel, P., & Smith, W. H. F. (1991). Free software helps map and display data. *Eos, Transactions American Geophysical Union*, *72*(41), 441–446. https://doi.org/10.1029/90eo00319

Wüstefeld, A., & Bokelmann, G. (2007). Null detection in shear-wave splitting measurements. *Bulletin of the Seismological Society of America*, *97*(4), 1204–1211. https://doi.org/10.1785/0120060190

Wyman, D. A. (2019). 2.8 Ga subduction-related magmatism in the Youanmi Terrane and a revised geodynamic model for the Yilgarn Craton. *Precambrian Research*, *327*, 14–33. https://doi.org/10.1016/j.precamres.2019.02.008

Wyman, D. A., & Kerrich, R. (2009). Plume and arc magmatism in the Abitibi subprovince: Implications for the origin of Archean continental lithospheric mantle. *Precambrian Research*, *168*(1), 4–22. https://doi.org/10.1016/j.precamres.2008.07.008

Yoshizawa, K. (2014). Radially anisotropic 3-D shear wave structure of the Australian lithosphere and asthenosphere from multi-mode surface waves. *Physics of the Earth and Planetary Interiors*, *235*, 33–48. https://doi.org/10.1016/j.pepi.2014.07.008

Yoshizawa, K., & Kennett, B. L. N. (2015). The lithosphere-asthenosphere transition and radial anisotropy beneath the Australian continent. *Geophysical Research Letters*, *42*(10), 3839–3846. https://doi.org/10.1002/2015gl063845

Yuan, H., & Romanowicz, B. (2010). Lithospheric layering in the North American craton. *Nature*, *466*(7310), 1063–1068. https://doi.org/10.1038/nature09332

Yuan, H., Romanowicz, B., Fischer, K. M., & Abt, D. (2011). 3-D shear wave radially and azimuthally anisotropic velocity model of the North American upper mantle. *Geophysical Journal International*, *184*(3), 1237–1260. https://doi.org/10.1111/j.1365-246X.2010.04901.x

## Reference From the Supporting Information

Yuan, H., & Levin, V. (2014). Stratified seismic anisotropy and the lithosphere-asthenosphere boundary beneath eastern North America. *Journal of Geophysical Research: Solid Earth*, *119*(4), 3096–3114. https://doi.org/10.1002/2013jb010785